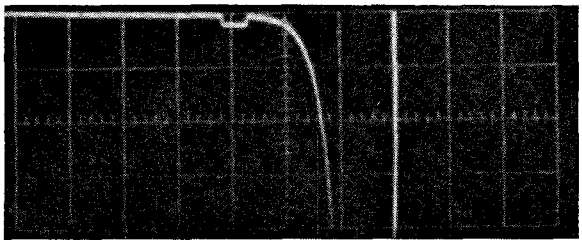

Fig. 8. Output of limiter showing low-power and high-power pulses.

Conclusions

It has been shown that the large signal nonlinear properties of ferroelectric materials can be used to obtain power limiting. A ferroelectric limiter capable of handling peak input power levels in excess of 25 kW, while yielding a saturated output power level of 300 watts with a small signal insertion loss of 0.5 dB has been built. A theoretical analysis, which accounts for the observed limiting action, indicates that power levels of several megawatts can be handled with suitably mounted ferroelectric pellets that can be conveniently fabricated. Even greater power handling capability can be expected if the ferroelectric material is used in a traveling-wave resonator configuration like that previously used to design a ferroelectric phase shifter.[4,5]

Additional data on the large signal properties of ferroelectric materials, particularly their temperature dependence, is needed. The limited available material data indicates that ferroelectric limiters will offer their greatest advantage in the HF, VHF, and UHF bands.

It should be noted that the structure used for the high-power ferroelectric limiter can readily be adopted for use as a high-power switch or an electronically tunable filter.

[4] Cohn, M., and A. F. Eikenberg, UHF ferroelectric phase shifter research, Res. Div. Electronic Communications, Inc., Timonium, Md., Final Rept on Contract No. AF 19(604)-8379, April 30, 1962.

[5] Cohn, M., and A. F. Eikenberg, Ferroelectric phase shifters for VHF and UHF, *IRE Trans. on Microwave Theory and Techniques*, vol MTT-10, Nov 1962, pp 536–548.

E- and *H*-Plane Bends for High-Power Oversized Rectangular Waveguide

JOHN P. QUINE, MEMBER, IEEE

Abstract—A study is presented of theoretical and experimental results of *E*- and *H*-plane bends for high-power oversized rectangular waveguide having cross-section dimensions in the range between 1.5 and 2.5 free space wavelengths. It is expected that waveguides having these dimensions will be able to transmit 50 to 100 kW of average power at *X*-band without water cooling. The transmission of at least 5.0 MW of peak power at *X*-band without pressurization is also a design objective.

Dimensions for bends having low-mode conversion loss were determined by numerical integration of the coupled transmission line equations. The dominant $TE_{10}^{\square}$ mode and four spurious modes were considered in these calculations. The results obtained for both constant curvature and sinusoidally shaped *E*- and *H*-plane bends are presented.

A compact *H*-plane constant curvature bend is described for which the ratio of centerline radius to waveguide width is equal to 1.48. The measured mode conversion loss to the $TE_{20}^{\square}$, $TE_{30}^{\square}$, and $TE_{40}^{\square}$ modes for an experimental model having a width equal to 2.25 inches was less than −20 dB in the frequency range from 7.0 to 11.0 Gc/s.

Manuscript received June 15, 1964; revised November 2, 1964. The work was supported by the Rome Air Development Center under Contract AF 30(602)-2990 with the General Electric Company, Heavy Military Electronics Department.

The author is with Advanced Technology Laboratories, General Electric Company, Schenectady, N. Y.

Introduction

THE PRACTICAL realization of reliable oversized waveguide systems for high-power applications depends on the development of components having low-energy conversion to spurious propagating modes. An important advantage of rectangular waveguide in the design of components, such as bends, is the absence of modes which are degenerate with the desired $TE_{10}^{\square}$ mode. The bend study outlined here is part of a general study to develop a whole family of components compatible with rectangular waveguides of the stated dimensions.

Dimensions for bends having low-mode conversion loss were determined by numerical integration of the coupled transmission line equations. The dominant $TE_{10}^{\square}$ mode and four spurious modes were considered in these calculations. Theoretical results are presented for both constant curvature and sinusoidally shaped *E*- and *H*-plane bends. Experimental results are presented for constant curvature *H*-plane bends.

Constant Curvature Bends

A waveguide bend can be represented by *n*-coupled

transmission lines, n being the number of propagating modes. The normalized coupled mode voltages E_n are related by the following set of simultaneous differential equations:

$$\begin{aligned}
&\frac{dE_1}{dz} + k_{11}E_1 + k_{12}E_2 + \cdots + k_{1n}E_n = 0\\
&\frac{dE_2}{dz} + k_{12}E_1 + k_{22}E_2 + \cdots + k_{2n}E_n = 0\\
&\cdots\cdots\cdots\cdots\cdots\cdots\\
&\frac{dE_n}{dz} + k_{1n}E_1 + k_{2n}E_2 + \cdots + k_{nn}E_n = 0
\end{aligned} \tag{1}$$

In (1), k_{nn} is the propagation constant for the mode n, and k_{mn} is the coupling coefficient between the modes m and n. The distance z is measured along the centerline of the bend. The coupling coefficients can be derived by an electromagnetic analysis [2], [4], [5].

If it is assumed that the power in all modes, except modes 1 and 2, is negligible, relatively simple closed-form solutions can be obtained for (1) for the case of constant curvature bends. This case has been studied in detail by Miller [1], who considered a system of two coupled transmission lines, and showed that the coupling causes the power to transfer cyclically between the two coupled modes along the coupling region. This principle can be used to design waveguide bends. Thus, bend dimensions can be adjusted so that power which is incident in mode one couples over to some degree to mode two, and then couples back to mode one. Similarly, bend dimensions can be adjusted to obtain any number of cycles of power transfer between modes.

If unit power is incident in mode one at the input of a bend of constant curvature ($z=0$), the magnitude of the normalized voltage, for mode two at any point z along the bend [1] is given by

$$|E_2| = \frac{\sin [Ak_{12}z]}{A} \tag{2}$$

where

$$A = \sqrt{\left(\frac{k_{11} - k_{22}}{2k_{12}}\right)^2 + 1} \tag{3}$$

It can be seen that the power in mode two has zero or maximum values at points along the coupling region corresponding to values of $Ak_{12}z$ equal to even or odd mutiples of $\pi/2$, respectively. The maximum power that can be transferred to mode two is given by

$$P_{2\max} = \frac{1}{A^2} = \frac{1}{\left(\frac{k_{11} - k_{22}}{2k_{12}}\right)^2 + 1} \tag{4}$$

Thus, if the two coupled modes are degenerate ($k_{11}=k_{22}$), $P_{2\max}$ is equal to unity. On the other hand, if $(k_{11}-k_{22})^2$ is very much greater than $(2k_{12})^2$, $P_{2\max}$ is very small.

For an H-plane bend excited by an incident $TE_{10}^{\square}$ mode, the propagation constants and coupling coefficients occurring in (1) are given by

$$k_{mn} = -j\frac{4mn}{(m^2-n^2)^2\pi^2}\left(\frac{a}{R}\right)\sqrt{\beta_m\beta_n}\left\{1 + \left(\frac{\beta^2}{\beta_m\beta_n}\right)\left[1 - \frac{(m^2+n^2)}{8}\left(\frac{\lambda}{a}\right)^2\right]\right\} \tag{5}$$

$$k_{mn} = \beta_m = \beta\sqrt{1 - \left(\frac{m\lambda}{2a}\right)^2} \tag{6}$$

$$\beta = 2\pi/\lambda \tag{7}$$

In (5) to (7), a is the waveguide width, b is the waveguide height, λ is the free space wavelength, and R is the radius of curvature of the bend centerline. The expression for k_{mn} given by (5) was derived by a method attributed to Schelkunoff [2], [4], [5], and represents the coupling coefficient between the $TE_{mo}^{\square}$ and $TE_{no}^{\square}$ modes, provided $m-n$ is odd. If $m-n$ is even, k_{mn} is zero. Thus, coupling occurs directly between an incident $TE_{10}^{\square}$ mode and all of the $TE_{no}^{\square}$ modes for which n is even. The even order $TE_{mo}^{\square}$ modes in turn couple directly to all of the $TE_{no}^{\square}$ modes for which n is odd. Power in an incident $TE_{10}^{\square}$ mode, therefore, is coupled directly or indirectly to all of the $TE_{no}^{\square}$ modes.

Theoretical and experimental data for constant curvature H-plane bends are shown in Fig. 1 for several values of bend angle and cycles of power transfer. These curves give the value of the centerline radius, R, which results in zero power in the $TE_{20}^{\square}$ mode at the bend output with a $TE_{10}^{\square}$ mode incident at the bend input. The theoretical data were obtained from solutions of the coupled transmission line equations. The solid curves represent the first-order closed-form approximation obtained by assuming that only the $TE_{10}^{\square}$ and $TE_{20}^{\square}$ modes have significant power. In this case, the solutions for R/a were obtained from (2) by setting $Ak_{12}z$ equal to $N\pi$, and z equal to $2R\alpha$, where N is the number of cycles of power transfer along the bend, and 2α is the total bend angle.

The computer results given in Fig. 1 were obtained by numerical integration of (1) considering the effects of all forward propagating modes up to and including the $TR_{50}^{\square}$ mode. These data were obtained by plotting the calculated values of E_{20} as a function of R/a (or a/λ) with a/λ (or R/a) held constant in order to determine the values of R/a (or a/λ) that would result in a zero value of E_{20}. The results are listed in Table I. Within the accuracy of these graphic calculations, the values of R/a and a/λ resulting in zero values for E_{20} were the same for both the 45° one-cycle bends and the 90° two-cycle bends. The two computer points for the lower pair of curves in Fig. 1, which are marked one-cycle 90° or two-cycle 180°, were calculated only for the case of the one-cycle 90° bends.

The fact that the curves in Fig. 1 first rise and then

fall to zero with increasing values of a/λ indicates that for a particular value of R/a there are two values of a/λ for which the conditions for zero $TE_{20}^{\square}$ mode power at the bend output are satisfied. At frequencies corresponding to these two values of a/λ, the mode conversion from the $TE_{10}^{\square}$ mode to the $TE_{20}^{\square}$ mode would be exactly zero. Low-mode conversion from the $TE_{10}^{\square}$ mode to the $TE_{20}^{\square}$ mode, therefore, can be obtained over a broad frequency range by operating near the maxima of the curves in Fig. 1. However, these curves do not give any information concerning the level of the higher order spurious modes such as the $TE_{30}^{\square}$, $TE_{40}^{\square}$, and $TE_{50}^{\square}$ modes. Calculated voltages for these modes at the bend output are given in Tables II and III. Inspection of these data and the data given in Table I indicates that mode conversion losses of less than one per cent can be expected over frequency bandwidths exceeding 5 per cent for a bend having $R/a=6.0$, if a/λ is centered about a value equal to 2.2. It appears likely that low-mode conversion loss over a 5 per cent frequency bandwidth also can be obtained for bends having $R/a=6.6$ if a/λ is centered about a value equal to 2.5.

The calculated values of the mode voltages given in the tables have cumulative integration errors which have been estimated to be less than ± 0.3 per cent. Because of these errors, the total mode conversion loss can be calculated more accurately from the sum of the squares of the spurious mode voltages than from the square of the dominant mode voltage.

In a very gradual bend of constant curvature, appreciable energy exists in only the $TE_{10}^{\square}$ and $TE_{20}^{\square}$ modes, and power is transferred periodically between these two modes along the length of the bend [1]. In this case, energy in the $TE_{20}^{\square}$ mode is a maximum at the center in the one-cycle bends, and at the quarter and three-quarter points in the two-cycle bends. The presence of the $TE_{20}^{\square}$ mode, however, provides a "tapered" source for excitation of the $TE_{30}^{\square}$ mode. The computer calculations indicate, however, that the positions of the $TE_{20}^{\square}$ mode maxima and minima along the bend are not greatly shifted by the presence of appreciable $TE_{30}^{\square}$ mode energy, and that the $TE_{30}^{\square}$ mode maxima and minima occur near the maxima and minima, respectively, of the $TE_{20}^{\square}$ mode. Figs. 2 and 3, and Table IV show typical computer results for one-cycle and two-cycle bends. In Fig. 2, bend angles of 45° and 90° correspond to normalized distances of 49.5 and 99, respectively, along the bend. In Fig. 3, bend angles of 45° and 90° correspond to normalized distances of 45 and 90, respectively, along the bend.

The voltages of the various modes at the point along a 90° bend at which the power in the $TE_{20}^{\square}$ mode has its maximum value are given in Table IV. The maximum values of E_{mo} occurring at any point along the bend are given in parentheses beneath the values of E_{mo} occurring at the points of maximum E_{20}. The data for the 45° bends are essentially the same as for the 90° bends.

The power which is converted to the $TE_{20}^{\square}$ mode within the bend results in increased dissipation per unit length, and reduced peak power handling capability compared to that of straight waveguide of the same dimensions carrying the $TE_{10}^{\square}$ mode. It can be shown that the $TE_{10}^{\square}$ and the $TE_{20}^{\square}$ modes are nearly in phase at the points of maximum E_{20} along the bend, with constructive interference between the fields of the two modes occurring for radii greater than R.

Theoretical data are shown in Figs. 4 and 5 for constant curvature E-plane bends. These curves give the value of the centerline radius, R, which results in zero power in the $TE_{11}^{\square}$, $TM_{11}^{\square}$ degenerate mode pair. In calculating the solid curves in these figures, it was assumed that only the incident $TE_{10}^{\square}$ mode and the $TE_{11}^{\square}$, $TM_{11}^{\square}$ degenerate mode pair have significant power. The coupling coefficient, k_{01}, between these modes was substituted for k_{12} in (2), and $Ak_{12}z$ was set equal to $N\pi$. An expression for k_{01} can be obtained by setting $n=1$ in the following, more general expressions for k_{on}, the coupling coefficient between the $TE_{10}^{\square}$ mode and the $TE_{1n}^{\square}$, $TM_{1n}^{\square}$ degenerate mode pair.

$$k_{on} = \sqrt{(k_{on}^{TE})^2 + (k_{on}^{TM})^2} \tag{8}$$

$$k_{on}^{TE} = -j \frac{\sqrt{2}b\beta_{1n}}{n^2\pi^2 R\sqrt{1+\left(\frac{na}{b}\right)^2}}\left[\sqrt{\frac{\beta_{10}}{\beta_{1n}}} + \sqrt{\frac{\beta_{1n}}{\beta_{10}}}\right] \tag{9}$$

$$k_{on}^{TM} = -j \frac{2\sqrt{2}a\beta}{n\pi^2 R\sqrt{1+\left(\frac{na}{b}\right)^2}} \cdot \left[\sqrt{\frac{\beta_{10}}{\beta_{1n}}} + \sqrt{\frac{\beta_{1n}}{\beta_{10}}}\right] \tag{10}$$

$$\beta_{1n} = \frac{2\pi}{\lambda}\sqrt{1-\left(\frac{\lambda}{2a}\right)^2 - \left(\frac{n\lambda}{2b}\right)^2} \tag{11}$$

The terms k_{on}^{TM} and k_{on}^{TM} given by (9) and (10) represent the coupling coefficients between the $TE_{10}^{\square}$ mode and the $TE_{1n}^{\square}$ and $TM_{1n}^{\square}$ modes, repectively, provided n is odd. For even values of n, k_{on}^{TE} and k_{on}^{TM} are each equal to zero. The ratio k_{on}^{TE}/k_{on}^{TM}, which approaches zero for large values of n or a/b, has exactly the value required to cause the total transverse electric field parallel to the b dimension in the bend to be zero for each degenerate mode pair. If (9) and (10) are substituted into (8), there results

$$k_{on} = -j\frac{\sqrt{2}b}{n^2\pi^2 R}\beta_{10}\left[\sqrt{\frac{\beta_{10}}{\beta_{1n}}} + \sqrt{\frac{\beta_{1n}}{\beta_{10}}}\right] \tag{12}$$

where the width a now occurs only in β_{10} and β_{1n}.

The values of R/a for one-cycle 45° or two-cycle 90° constant curvature E-plane bends are shown plotted vs. a/λ in Fig. 4 for several values of the aspect ratio, b/a. These data indicate that the value of R/b is

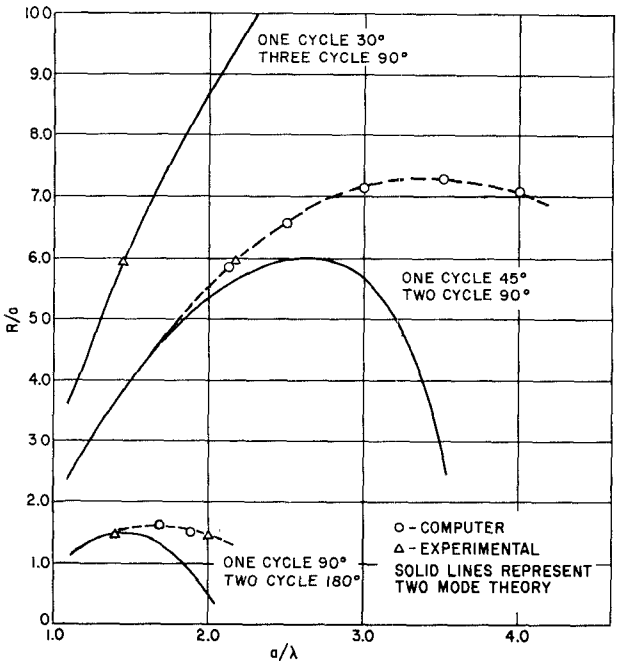

Fig. 1. Dimensions for $TE_{10}^{\square}$ mode constant curvature H-plane bends.

TABLE I

DIMENSIONS FOR H-PLANE BENDS RESULTING IN $E_{20}=0$

a/λ	R/a
45° one-cycle or 90° two-cycle bends	
2.12	5.83
2.15	5.90
2.20	6.00
2.50	6.60
3.00	7.10
3.50	7.23
4.00	7.04
90° one-cycle bends	
a/λ	R/a
1.66	1.60
1.88	1.50

equal to approximately 11 at the maxima of all the curves, and that the ratio b/a must be increased as a/λ is decreased.

The data plotted in Fig. 4 can be condensed into a single curve by plotting R/b as a function of b/λ_{10} where λ_{10} is the wavelength of the $TE_{10}^{\square}$ mode. Thus, all the curves of Fig. 4 are represented by the single solid curve for one-cycle 45° and two-cycle 90° bends shown in Fig. 5. Representation of the data with a single curve is made possible by the fact that the E-plane bend problem is essentially two-dimensional.[1] This can be seen from (12), which shows that k_{on} is a function of b/R and λ_{10}.

As stated in the foregoing, the solid curves in Fig. 4 and 5 were obtained by assuming that only the $TE_{10}^{\square}$

[1] This was correctly outlined in personal correspondence of A. A. L. Browne of the Lincoln Laboratory, Massachusetts Institute of Technology, Lexington, Mass.

TABLE II

COMPUTER CALCULATIONS FOR CONSTANT CURVATURE 90° H-PLANE BENDS

Mode Content at Bend Output*

a/λ	R/a	E_{10}	E_{20}	E_{30}	E_{40}	E_{50}
1.70	1.60	0.9961	0.0185	0.0835	—	—
1.80	1.50	0.9944	0.0670	0.0790	—	—
1.90	1.50	0.9983	0.0127	0.0508	—	—
2.12	5.90	0.9987	0.0355	0.0288	0.00339	—
2.25	5.90	0.9946	0.0962	0.0255	0.00107	—
2.28	5.90	0.9913	0.126	0.0218	0.00712	—
2.12	6.00	0.9962	0.0780	0.0359	0.00136	—
2.25	6.00	0.9980	0.0502	0.0257	0.00277	—
2.28	6.00	0.9961	0.0796	0.0229	0.00399	—
2.50	6.50	0.9989	0.0479	0.00312	0.00107	—
3.00	7.30	0.9976	0.0298	0.0986	0.00716	0.00132
3.50	7.20	0.9942	0.0320	0.1271	0.0252	0.00417
4.00	7.06	0.9970	0.01023	0.0601	0.0496	0.00608

* Mode power is proportional to $|E_{mo}|^2$.

TABLE III

COMPUTER CALCULATIONS FOR CONSTANT CURVATURE 45° H-PLANE BENDS

Mode Content at Bend Output*

a/λ	R/a	E_{10}	E_{20}	E_{30}	E_{40}	E_{50}
2.12	5.90	0.9994	0.0152	0.0254	0.00506	—
2.25	5.90	0.9976	0.0507	0.0414	0.00472	—
2.28	5.90	0.9967	0.0643	0.0457	0.00408	—
2.12	6.00	0.9989	0.0369	0.0247	0.00525	—
2.25	6.00	0.9986	0.0290	0.0389	0.00450	—
2.28	6.00	0.9979	0.0425	0.0429	0.00468	—
2.50	6.50	0.9980	0.0250	0.0581	0.00640	—
3.00	7.30	0.9901	0.0347	0.0879	0.00269	0.000856
3.50	7.20	0.9990	0.00921	0.0614	0.0366	0.00645
4.00	7.06	0.9984	0.00495	0.0209	0.0523	0.00809

* Mode power is proportional to $|E_{mo}|^2$.

and the $TE_{11}^{\square}$, $TM_{11}^{\square}$ spurious mode pair have significant power. This assumption is correct for values of b/λ_{10} which are less than 1.0. For values of b/λ_{10} greater than 1.0, the $TE_{12}^{\square}$, $TM_{12}^{\square}$ spurious mode pair can propagate in the bend, and these modes are excited by the $TE_{11}^{\square}$, $TM_{11}^{\square}$ spurious mode pair.

Since the curves for one-cycle 90° or two-cycle 180° bends in Fig. 5 lies almost entirely in the region below $b/\lambda_{10}=1.0$, (2) can be used to predict the values of E_{11}, the normalized mode voltage for the composite $TE_{11}^{\square}$, $TM_{11}^{\square}$ degenerate spurious mode pair. For the composite mode, the total electric field parallel to the waveguide b dimension is equal to zero. Fig. 6 shows calculated values of E_{11} as a function of b/λ_{10} for one-cycle 90° bends. These data were obtained by substituting the expression for k_{01} given by (12) for k_{12} in (2), and setting z equal to $R\pi/2$. The data indicate that low-mode conversion loss can be obtained over a substantial bandwidth with a compact E-plane bend having R/b equal to approximately 2.4, and with b/λ_{10} centered about 0.82. This value of b/λ_{10} corresponds to approximately twice the value usually employed for standard single mode waveguide.

The computer points, (1.5, 11.30), (1.75, 11.50), (2.0, 10.55), plotted in Fig. 5 were obtained graphically

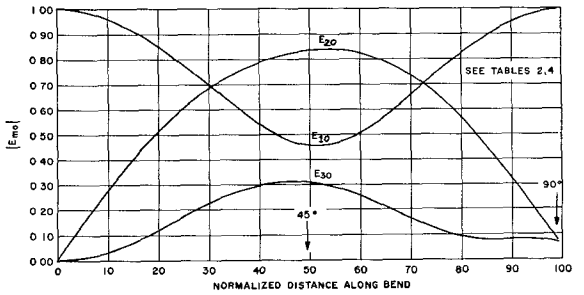

Fig. 2. Mode voltages along constant curvature H-plane bend ($R/a=1.5$, $a/\lambda=1.8$).

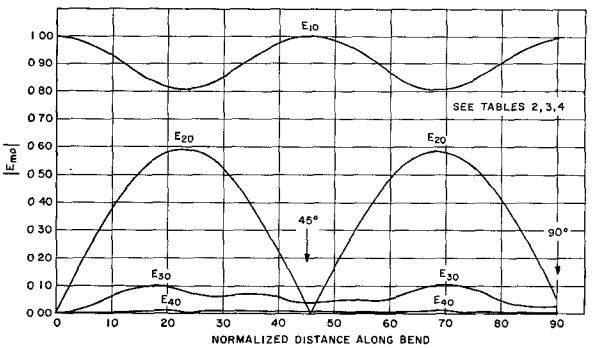

Fig. 3. Mode voltages along constant curvature H-plane bend ($R/a=6.0$, $a/\lambda=2.25$).

TABLE IV

COMPUTER CALCULATIONS FOR CONSTANT CURVATURE 90° H-PLANE BENDS

Mode Content at Point of Maximum E_{20}*

a/λ	R/a	E_{10}	E_{20}	E_{30}	E_{40}	E_{50}
1.70	1.60	0.5559	0.8094	0.1887 (0.2046)	—	—
1.80	1.50	0.4565	0.8379	0.299 (0.312)	—	—
1.90	1.50	0.3898	0.8322	0.3938 (0.3938)	—	—
2.12	5.90	0.8380	0.5422	0.0601 (0.0830)	0.00362 (0.00805)	—
2.25	6.00	0.8027	0.5901	0.0850 (0.1067)	(0.00718) (0.0110)	—
2.50	6.50	0.7707	0.6306	0.0918 (0.1427)	0.00363 (0.00854)	—
3.00	7.30	0.6213	0.7722	0.1469 (0.2461)	0.0241 (0.0368)	0.00433 (0.00559)
3.50	7.20	0.4548	0.8226	0.3407 (0.4137)	0.0737 (0.0955)	0.0105 (0.0175)
4.00	7.06	0.4050	0.7632	0.4804 (0.5901)	0.1489 (0.1941)	0.0275 (0.0357)

* Mode power is proportional to $|E_{mo}|^2$.

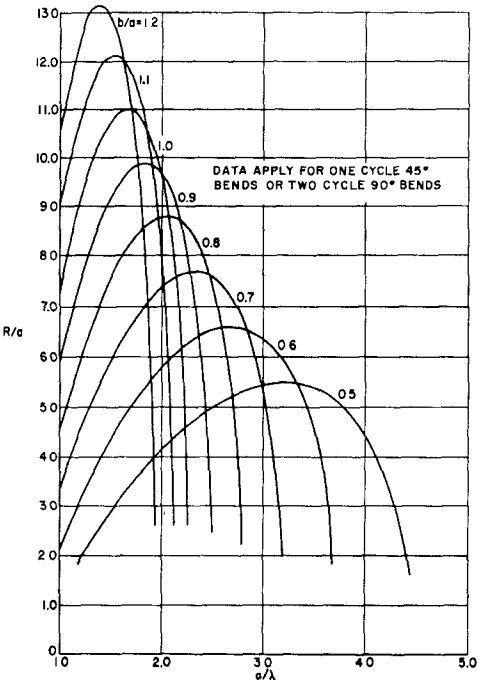

Fig. 4. Dimensions for $TE_{10}\square$ mode constant curvature E-plane bends.

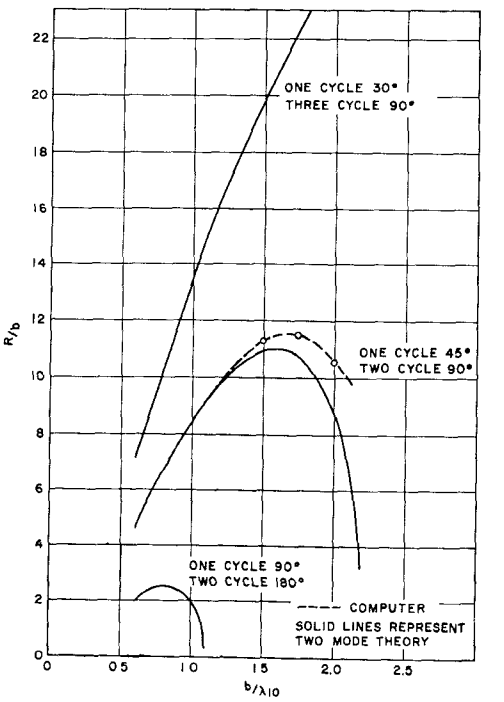

Fig. 5. Dimensions for $TE_{10}\square$ mode constant curvature E-plane bends.

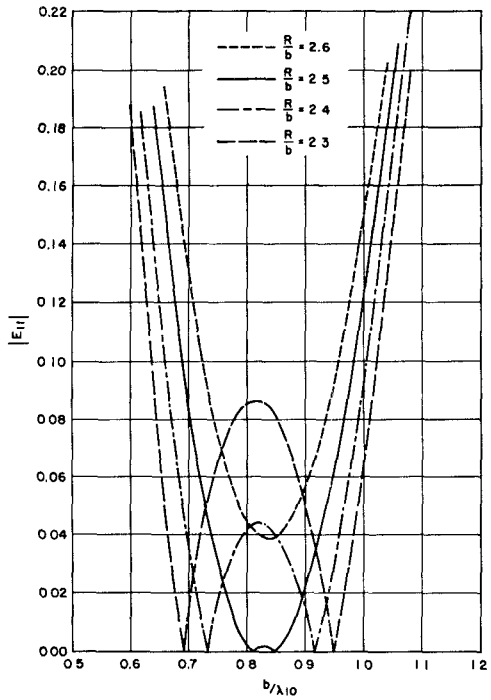

Fig. 6. Spurious mode voltage at output of 90° constant curvature E-plane bends.

TABLE V

COMPUTER CALCULATIONS FOR CONSTANT CURVATURE 90° E-PLANE BENDS

Mode Content at Bend Output*

b/λ_{10}	R/b	E_{10}	E_{11}	E_{12}	E_{13}
1.50	11.00	0.9979	0.0668	0.00167	—
1.50	11.50	0.9991	0.0432	0.00727	—
1.50	12.00	0.9891	0.1468	0.0180	—
1.75	10.90	0.9928	0.1204	0.00760	0.00160
1.75	11.10	0.9967	0.0815	0.00347	0.00782
1.75	11.30	0.9991	0.0425	0.00780	0.0124
2.00	11.00	0.9967	0.0719	0.0390	0.0102
2.00	11.50	0.9878	0.1445	0.0585	0.00893
2.00	12.00	0.9744	0.2133	0.0719	0.0129

* Mode power is proportional to $|E_{1n}|^2$.

TABLE VI

COMPUTER CALCULATIONS FOR CONSTANT CURVATURE 45° E-PLANE BENDS

Mode Content at Bend Output*

b/λ_{10}	R/b	E_{10}	E_{11}	E_{12}	E_{13}
1.50	11.0	0.9993	0.0331	0.0195	—
1.50	11.5	0.9997	0.0208	0.0173	—
1.50	12.0	0.9972	0.0731	0.0164	—
1.75	10.9	0.9981	0.0605	0.00285	0.0128
1.75	11.1	0.9991	0.0408	0.00143	0.0120
1.75	11.3	0.9998	0.0213	0.00360	0.00930
2.00	11.0	0.9974	0.0304	0.0654	0.00893
2.00	11.5	0.9961	0.0657	0.0577	0.0152
2.00	12.0	0.9933	0.1040	0.0498	0.0127

* Mode power is proportional to $|E_{1n}|^2$.

TABLE VII

COMPUTER CALCULATIONS FOR CONSTANT CURVATURE 90° E-PLANE BENDS

Mode Content at Point of Maximum E_{11}*

b/λ_{10}	R/b	E_{10}	E_{11}	E_{12}	E_{13}
1.50	11.00	0.7303	0.6808	0.0579 (0.0650)	—
1.50	11.30	0.7572	0.6518	0.0448 (0.0616)	—
1.50	11.50	0.7460	0.6642	0.0499 (0.0593)	—
1.50	12.00	0.7606	0.6479	0.0438 (0.0572)	—
1.75	10.90	0.5998	0.7961	0.0808 (0.1045)	0.0122 (0.0137)
1.75	11.10	0.6076	0.7904	0.0788 (0.1011)	0.0118 (0.0134)
1.75	11.30	0.6151	0.7846	0.0775 (0.1012)	0.00481 (0.0132)
2.00	11.00	0.5039	0.8547	0.1251 (0.1713)	0.00863 (0.0204)
2.00	11.50	0.4835	0.8639	0.1415 (0.1813)	0.0210 (0.0220)
2.00	12.00	0.5216	0.8449	0.1186 (0.1609)	0.00827 (0.1971)

* Mode power is proportional to $|E_{1n}|^2$.

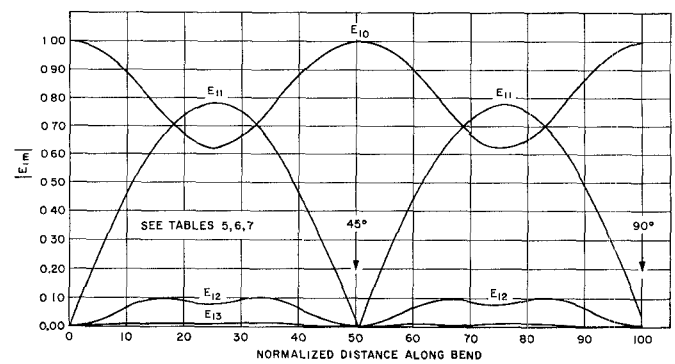

Fig. 7. Mode voltages along constant curvature E-plane bend ($R/b = 11.3$, $b/\lambda_{10} = 1.75$).

from the data given in Tables V and VI, and were essentially the same for both 45° one-cycle and 90° two-cycle bends. The data in Tables V and VI, and Fig. 5 indicate that low-mode conversion loss can be obtained for values of b/λ_{10} between 1.5 and 1.85 for 45° and 90° bends having R/b approximately equal to 11.3.

Table VII gives the mode voltage at the point along a 90° E-plane bend at which the E_{11} composite mode has its maximum value. The maximum values of E_{1n} occurring at any point along the bend are given in parentheses beneath the values of E_{1n} occurring at the points of maximum E_{11}. The data for 45° bends are essentially the same as for the 90° bends. Figure 7 shows the mode voltages along a constant curvature E-plane bend having $b/\lambda_{10} = 1.75$, and $R/b = 11.3$. In Fig. 7, bend angles of 45° and 90° correspond to normalized distances of 50 and 100, respectively, along the bend. It can be shown that the $TE_{10}^{\square}$ mode and the $TE_{11}^{\square}$, $TM_{11}^{\square}$ composite mode are nearly in phase at the points of maximum E_{11}, with constructive interference occurring between the fields of the two modes for radii greater than R.

Experimental Results

Measured data obtained at X-band are shown in Fig. 8 for an experimental H-plane constant curvature bend having R/a equal to 1.48. The ordinate, P_{mo}/P_{10} represents the ratio of the power in the $TE_{mo}^{\square}$ mode at the bend output to the power in the incident $TE_{10}^{\square}$ mode. The width, a, for this bend was 2.25 inches, and the height, b, was 0.497 inch. The results, however, apply for any other value of b. A 10-inch straight taper was employed to transform from the standard 1.122 by 0.497 inch waveguide to the oversized waveguide.

Mode conversion from the $TE_{10}^{\square}$ mode to each of the propagating modes in the bend was measured by a cavity method employing a movable short circuit [3]. The movable short circuit was of the spring finger type with contact made along the top and bottom walls. The residual spurious mode level with the 10-inch straight taper and the movable short circuit was below -30 dB over the entire frequency range of the measurements.

As a check on the cavity measurements, the mode conversion to the $TE_{20}^{\square}$ mode also was measured by a coupler method, and these data are shown as a solid line in Fig. 8. The coupler consisted of a single round hole centered on the top wall of an oversized waveguide section, and was employed to measure the ratio of the even-mode currents ($TE_{20}^{\square}$, $TE_{40}^{\square}$) to the odd-mode currents ($TE_{10}^{\square}$, $TE_{30}^{\square}$) at the bend output with the bend terminated in a 5-inch tapered absorbing load. Over most of the frequency range of the measurements, this ratio was approximately equal to the ratio of the $TE_{20}^{\square}$ mode current to the TE_{10} mode current. The residual even-mode level with the coupler method (10-inch taper, coupler, and absorbing load) was below -30 dB over the entire frequency range of the measurements, except near 10.5 Gc/s, which is equal to the cutoff frequency of the $TE_{40}^{\square}$ mode. Near this frequency, the residual even-mode level increased to -26 dB.

The data in Fig. 8 indicate reasonably good agreement between the two methods at all frequencies except near 10.5 Gc/s, where apparently a load mismatch occurred for the $TE_{40}^{\square}$ mode with the coupler method. It was noted that, with the bend in place, the coupler output due to the even-mode currents peaked up near this frequency at load positions spaced at intervals of one-half wavelength for the $TE_{40}^{\square}$ mode. Being near cutoff, the $TE_{40}^{\square}$ mode excited by the bend apparently was not well-absorbed by the tapered load. The fact that these even-mode resonances were observed less strongly when the bend was removed indicates that the $TE_{40}^{\square}$ mode was only weakly excited in this case.

The data of Fig. 8 show the broad frequency bandwidth predicted by the one-cycle curve of Fig. 1. Very-low-mode conversion loss was measured at frequencies near 7.5 Gc/s and 10.5 Gc/s, and these results provide the two experimental points for the one-cycle 90° curve of Fig. 1.

A second experimental H-plane constant curvature bend was also tested, and the results are shown in Fig.

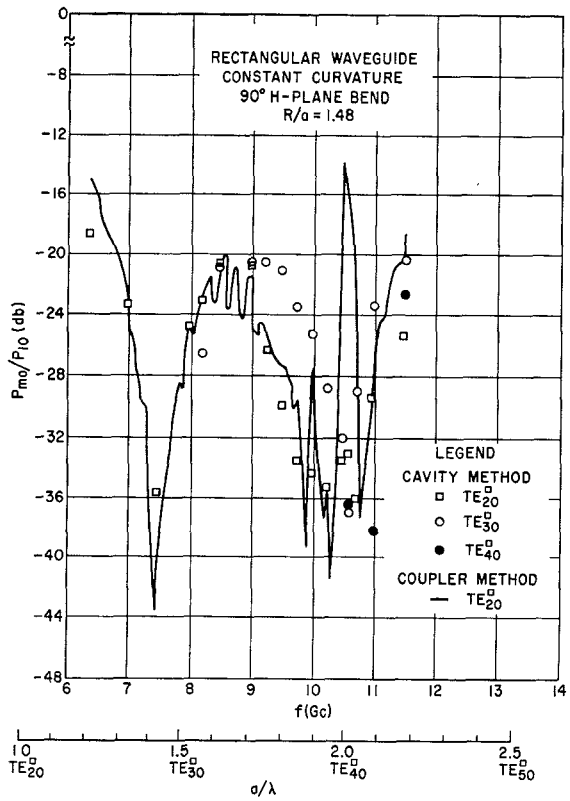

Fig. 8. Experimental results for H-plane bend.

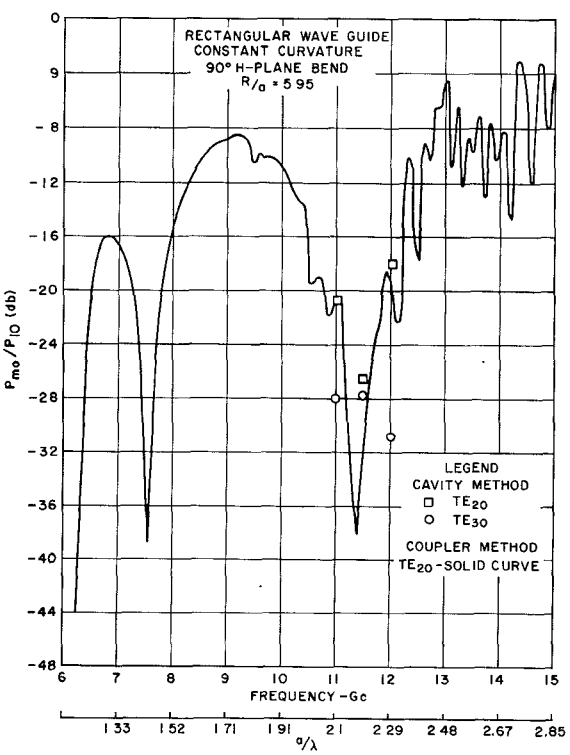

9. Experimental results for H-plane bend.

9. In this case, the width, a, and height, b, were equal to 2.25 and 0.497 inches, respectively, and the value of R/a was equal to 5.95. Measured mode conversion loss for this bend was low at the two values of a/λ indicated by the experimental points on the three- and two-cycle curves of Fig. 1. The measured data indicate that the level of all spurious modes is below −24 dB over approximately a 5 per cent bandwidth centered about the experimental point on the two-cycle curve of Fig. 1.

Measurements also were performed to determine the level of the spurious modes reflected from the bend input. These measurements were made with the even-odd mode coupler placed at the bend input, and with the 5-inch tapered absorbing load placed at the bend output. In the case of the bend having R/a equal to 1.48, the level of the reflected TE_{20}□ mode was below −40 dB for all frequencies up to 9.0 Gc/s, and below −30 dB up to 10.4 Gc/s which was the highest test frequency. In the case of the bend having R/a equal to 5.95, the coupler measurements indicated that the reflected TE_{20}□ mode was below −30 dB over approximately a 6 per cent bandwidth centered about the experimental point on the two-cycle curve of Fig. 1. This bandwidth probably was limited by spurious resonances associated with the coupler method.

The reflection coefficient for the dominant TE_{10}□ mode for the bend having $R/a = 1.48$ was determined by measuring the VSWR at the input to the 10-inch taper feeding the bend and tapered absorbing load. The measured VSWR was below 1.03 over the frequency range from 7.0 to 12.5 Gc/s. Measurements of the insertion loss to the TE_{10}□ mode also were performed on the bend having $R/a = 1.48$. The results were consistent with the measured mode conversion losses.

Bends with Variable Curvature

Bends having a variable radius of curvature also were investigated. The advantages of this approach have been demonstrated previously in the design of tapers for circular waveguides carrying the TE_{01}° mode [4], [5]. In this case, the cone angle was varied gradually along the length of the taper. It was thought that by gradually varying the radius of curvature in the bend case, it might be possible to obtain low-mode conversion loss over wider frequency ranges.

A computer program was developed for obtaining numerical solutions of (1) for the case in which the coupling coefficients vary along the length of the bend. Figure 10 shows the important dimensions for sinusoidally shaped E- or H-plane bends, and Tables VIII and IX indicate some initial results of computer calculations for the normalized mode voltages at the bend output for power incident in the TE_{10}□ mode. Inspection of these data also indicates that reasonably compact variable curvature H-plane bends can be designed. The dimensions for the E-plane bends are less compact because of the smaller differences in the propagation constants between the desired TE_{10}□ mode and the TE_{11}□, TM_{11}□ spurious mode pair.

The data in Table IX for the E-plane bends were calculated for an infinite waveguide width. In this case, the coupling coefficient, k_{on}, between the TEM mode and the TM_{on} mode in the resulting parallel plate waveguide is given by the following equation for odd values of n.

$$k_{on} = -j\frac{\sqrt{2}b}{n^2\pi^2 R}\left[\sqrt{\frac{\beta}{\beta_n}} + \sqrt{\frac{\beta_n}{\beta}}\right] \tag{13}$$

$$\beta_n = \beta\sqrt{1 - \left(\frac{n\lambda}{2b}\right)^2} \tag{14}$$

For even values of n, k_{on} is equal to zero. The coupling

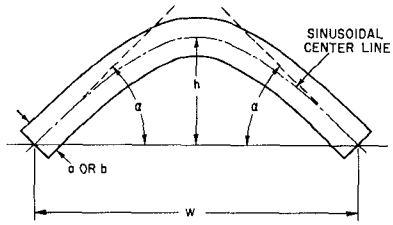

Fig. 10. Dimensions for sinusoidally shaped bends. a = width of H-plane bend; b = height of E-plane bend; $h = W/\pi \tan \pi$.

TABLE VIII

Computer Calculations for Sinusoidally Shaped 90° H-Plane Bends

Mode Content at Bend Output*

w/a	E_{10}	E_{20}	E_{30}	E_{40}	E_{50}
			$a/\lambda = 1.75$		
7.00	0.9985	0.0549	0.000759	—	—
8.00	0.9967	0.0815	0.000737	—	—
			$a/\lambda = 2.25$		
4.40	0.9918	0.0536	0.1159	0.00621	—
7.00	0.9914	0.1293	0.0169	0.000230	—
8.00	0.9966	0.0821	0.00602	0.000101	—
8.88	0.9995	0.0297	0.00112	0.000173	—
			$a/\lambda = 2.75$		
10.0	0.9872	0.1590	0.0128	0.000146	0.0000110
12.0	0.9999	0.0109	0.000742	0.000115	0.000000856
15.0	0.9983	0.0591	0.00133	0.000115	0.00000545

* Mode power is proportional to $|E_{mo}|^2$.

TABLE IX

Computer Calculations for Sinusoidally Shaped 90° E-Plane Bends

Mode Content at Bend Output*

w/b	E_{00}	E_{01}	E_{02}	E_{03}
		$b/\lambda = 1.5$		
20.0	0.9999	0.0184	0.000121	—
		$b/\lambda = 2.0$		
20.0	0.9981	0.0624	0.00885	0.000273
40.0	0.9983	0.0621	0.000131	0.0000383
60.0	0.9986	0.0253	0.0000265	0.0000163

* Mode power is proportional to $|E_{on}|^2$.

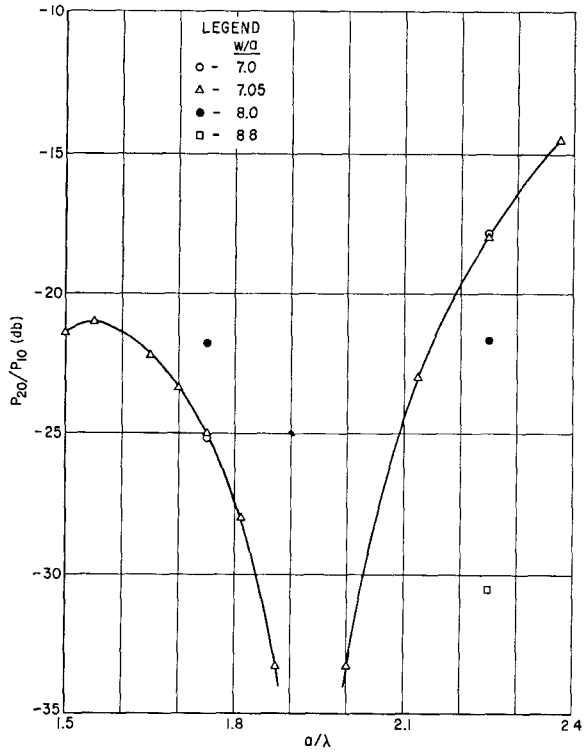

Fig. 11. Calculated values of output power in $TE_{20}\square$ mode for 90° sinusoidally shaped H-plane bends.

coefficients between the TM_{on} mode and the TM_{om} mode in parallel plate waveguide are given by the following equation for odd values of $m-n$.

$$k_{mn}=-j\frac{2b\beta}{(m^2-n^2)^2\pi^2R}\left\{(m^2+n^2)\sqrt{\frac{\beta_n\beta_m}{\beta^2}}+\left(m^2+n^2-\frac{m^2n^2\lambda^2}{2b^2}\right)\sqrt{\frac{\beta^2}{\beta_n\beta_m}}\right\} \quad (15)$$

If $m-n$ is even, k_{mn} is equal to zero. For a finite waveguide width, the free space wavelength, λ, should be replaced with λ_{10}, the wavelength of the $TE_{10}\square$ mode. It can be seen that in this case (13) becomes identical to (12).

Calculated voltages for the $TE_{20}\square$ mode at the output of sinusoidally shaped H-plane bends are shown plotted as a function of a/λ in Fig. 11. For the case $w/a=7.05$ (Fig. 10), these data indicate that the $TE_{20}\square$ mode voltage is below -30 dB over a 10 per cent bandwidth centered near $a/\lambda=1.93$, and that a maximum for the $TE_{20}\square$ mode voltage occurs at $a/\lambda=1.55$. Although not calculated for lower values of a/λ, the $TE_{20}\square$ mode voltage probably oscillates with decreasing maxima as a/λ is decreased. The positions of the plotted points for other values of w/a in Fig. 11 indicate that the frequency for zero $TE_{20}\square$ mode voltage increases as w/a is increased.

The mode voltages at the bend output and at the point of maximum E_{20} are given in Tables X and XI, respectively. Fig. 12 shows how the mode voltages vary

TABLE X

COMPUTER CALCULATIONS FOR SINUSOIDALLY SHAPED 90° H-PLANE BENDS

Mode Content at Bend Output*
$w/a=7.05$

a/λ	E_{10}	E_{20}	E_{30}	E_{40}	E_{50}
1.500	0.9964	0.0852	—	—	—
1.550	0.9960	0.0897	0.000226	—	—
1.600	0.9965	0.0847	0.000123	—	—
1.650	0.9971	0.0772	0.000522	—	—
1.700	0.9978	0.0676	0.000721	—	—
1.750	0.9985	0.0563	0.000784	—	—
1.8125	0.9993	0.0400	0.000841	—	—
1.875	0.9998	0.0216	0.000997	—	—
2.000	0.9998	0.0218	0.00264	—	—
2.125	0.9975	0.0707	0.00833	0.000148	—
2.250	0.9918	0.1269	0.0160	0.000171	—
2.375	0.9818	0.1884	0.0245	0.000577	—
2.500	0.9669	0.2535	0.0325	0.000797	—
2.625	0.9469	0.3193	0.0396	0.000805	0.0000300
2.750	0.9217	0.3855	0.0447	0.00283	0.0000551

* Mode power is proportional to $|E_{mo}|^2$.

TABLE XI

COMPUTER CALCULATIONS FOR SINUSOIDALLY SHAPED 90° H-PLANE BENDS

Mode Content at Point of Maximum E_{20}*
$w/a=7.05$

a/λ	E_{10}	E_{20}	E_{30}	E_{40}	E_{50}
1.500	0.9425	0.3342	—	—	—
1.550	0.9320	0.3618	0.0238	—	—
1.600	0.9232	0.3829	0.0347	—	—
1.650	0.9127	0.4064	0.0431	—	—
1.700	0.9012	0.4303	0.0524	—	—
1.750	0.8868	0.4579	0.0635	—	—
1.8125	0.8717	0.4841	0.0768	—	—
1.875	0.8563	0.5085	0.0903	—	—
2.000	0.8232	0.5554	0.1183	—	—
2.125	0.7710	0.6210	0.1700	0.0210	—
2.250	0.7326	0.6443	0.2173	0.0309	—
2.375	0.6778	0.6841	0.2656	0.0446	—
2.500	0.6277	0.7138	0.3053	0.0575	—
2.625	0.5863	0.7337	0.3363	0.0698	0.00965
2.750	0.5564	0.7450	0.3592	0.0787	0.0120

* Mode power is proportional to $|E_{mo}|^2$.

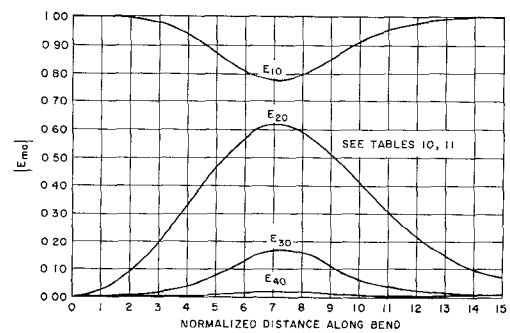

Fig. 12. Mode voltages along sinusoidally shaped 90° H-plane bend ($W/a=7.05$, $a/\lambda=2.125$).

along the length of a sinusoidally shaped H-plane bend having $w/a = 7.05$ and $a/\lambda = 2.125$. The computer calculations indicate that for reasonably gradual bends the spurious mode voltages along the sinusoidally shaped bends increase monotonically from the bend input to the bend center, and then decrease monotonically from the bend center to the bend output. This variation should be compared with the cyclic variation obtained with the constant curvature bends.

Conclusions

The theoretical and experimental results indicate that reasonably compact constant curvature and variable curvature bends can be designed for rectangular waveguides having cross-section dimensions in the range between 1.5 and 2.5 free space wavelengths. Calculations indicate that low-mode conversion loss can be obtained over broad frequency bandwidths with the sinusoidally shaped bends.

The close agreement between the experimental and computer data indicates that accurate results can be expected with the calculated coupling coefficients and the coupled transmission line equations, provided all forward propagating modes are considered.

Acknowledgments

The author is pleased to acknowledge the valuable contributions of C. Younger in the experimental phases of this work. He also wishes to express his thanks to H. W. Moore for his efforts in programming the computer calculations, and to G. E. Feiker, E. S. Sampson, K. Tomiyasu, R. D. Wengenroth, and V. Vannicola for many helpful discussions.

References

[1] Miller, S. E., Coupled wave theory and waveguide applications, *Bell Sys. Tech. J.*, vol 33, May 1954, pp 661–720.
[2] Schelkunoff, S. A., Conversion of Maxwell's equations into generalized telegraphist's equations, *Bell Sys. Tech. J.*, vol 34, Sep 1955, pp 995–1043.
[3] Klinger, Y., The measurement of spurious modes in over-moded waveguides, *Proc. IEEE, pt B Suppl.*, Jan 1959, pp 89–99.
[4] Unger, H. G., Circular waveguide taper of improved design, *Bell Sys. Tech. J.*, vol 37, Jul 1958, pp. 899–912.
[5] Tang, C. C. H., Optimization of waveguide tapers capable of multimode operation, *IRE Trans. on Microwave Theory and Techniques*, vol MTT-9, Sep 1961, pp 442–452.

Microwave Delay Techniques Using YIG

F. A. OLSON AND J. R. YAEGER

Abstract—**Recent developments in microwave delay techniques employing single-crystal yttrium iron garnet (YIG) are described. In particular, the operation of a two-port, electronically variable-delay device utilizing long-wavelength spin-wave propagation in single-crystal YIG is presented in detail. Specific advantages of this device are transmission-type operation, delay continuously variable from zero to several microseconds by means of magnetic field, and lack of critical dimensions or surface finishes. This form of delay, as well as those due to acoustic-wave and spin-wave/acoustic-wave propagation, have been observed at frequencies from 1 to 10 Gc/s. A comparison of the performances of these delay processes is made, with special attention to insertion loss, bandwidth, frequency limits, and variable-delay range.**

Introduction

THE ABILITY to delay microwave signals and, in particular, to control the delay electronically, is important to certain electronic systems. There has been considerable activity in this field recently, with the most significant noncryogenic results being achieved through the use of various delay processes in single-crystal yttrium iron garnet (YIG). A number of favorable conditions and phenomena suitable for microwave delay applications exist in a ferrimagnetic material such as YIG. The small magnetic loss in YIG is of particular interest here in that it allows reasonably efficient generation and propagation of magnetostatic waves and spin waves [1], [2]. This paper is mainly concerned with the application of long-wavelength spin waves (magnetostatic waves) to accomplish continuously variable delay [3]. The operation of this delay unit is compared with two other types of operation in YIG: fixed delay using low-loss acoustic waves [4], [5], and variable delay using combinations of acoustic and spin waves [6]. Special attention is given to delay range, insertion loss, bandwidth, and frequency limits of the delay processes.

Manuscript received September 29, 1964; revised October 30, 1964.
The authors are with the Microwave Electronics Corp., Palo Alto, Calif.

Variable Delay Utilizing Magnetostatic Waves

The propagation of magnetostatic waves in a longitudinally magnetized rod of YIG has been used to accomplish microwave variable delay. The magnetic waves result from the transverse microwave magnetic field applied at the end region of the YIG rod. The mag-